

# PCCP

Accepted Manuscript



This is an *Accepted Manuscript*, which has been through the Royal Society of Chemistry peer review process and has been accepted for publication.

*Accepted Manuscripts* are published online shortly after acceptance, before technical editing, formatting and proof reading. Using this free service, authors can make their results available to the community, in citable form, before we publish the edited article. We will replace this *Accepted Manuscript* with the edited and formatted *Advance Article* as soon as it is available.

You can find more information about *Accepted Manuscripts* in the [Information for Authors](#).

Please note that technical editing may introduce minor changes to the text and/or graphics, which may alter content. The journal's standard [Terms & Conditions](#) and the [Ethical guidelines](#) still apply. In no event shall the Royal Society of Chemistry be held responsible for any errors or omissions in this *Accepted Manuscript* or any consequences arising from the use of any information it contains.



## Physical Chemistry Chemical Physics

## ARTICLE

## Structural analysis of bioinspired nano materials with synchrotron Far IR spectroscopy

Rania S. Seoudi<sup>a</sup>, Annette Dowd<sup>b</sup>, Brian J. Smith<sup>a</sup>, Adam Mechler<sup>a</sup>

Received 00th January 20xx,  
Accepted 00th January 20xx

DOI: 10.1039/x0xx00000x

www.rsc.org/

Bioinspired fibres and hierarchical nano-materials are based on the self-assembly of organic building blocks such as polypeptides. Confirming the core structure of such materials is often challenging as they lack the long-range order required by crystallographic methods. Far-IR spectroscopy characterizes the vibrational modes of large molecular units. These vibrational modes are very sensitive to angle strain and second order interactions such as hydrogen bonding. As such, far-IR spectra hold information about the secondary structure and interactions of large biomolecules. Here we analyze the far-IR vibrational spectra of fibrous nano-materials based on three isomeric unnatural tripeptides, Ac- $\beta^3$ Leu- $\beta^3$ Ile- $\beta^3$ Ala, Ac- $\beta^3$ Ile- $\beta^3$ Ala- $\beta^3$ Leu, and Ac- $\beta^3$ Ala- $\beta^3$ Leu- $\beta^3$ Ile. These peptides have well described self-assembly characteristics, forming one-dimensional nanorods that impose tight conformational constraints on the constituent molecules. The synchrotron far-IR spectroscopic results were interpreted by using density functional theory (DFT) modelling based vibrational analysis. The sensitivity of the spectra to peptide conformation was assessed by comparing the experimental spectra with DFT predictions. In high dielectric implicit solvent, intramolecular hydrogen-bonding is inhibited and thus the energy minimized peptide structure remains close to the 14-helix folding characteristic of substituted  $\beta^3$ -peptides, giving good agreement between the experimental and predicted vibration spectra. In contrast, energy minimization in vacuum alters the peptide conformation leading to intramolecular hydrogen bonds, and hence the predicted vibration spectra do not agree with the experimental data. Therefore, our results demonstrate the ability of far-IR spectroscopy to identify correct structural predictions and thus open the way for using far-IR spectroscopy for the characterization and structural analysis of bioinspired nano-materials and potentially their interactions with surfaces, ionic environments and other biomolecules. Far-IR structural analysis is particularly powerful in case of one- and two-dimensional materials such as fibres, hydrogels and thin layers where standard crystallographic analysis is not available.

### 1 Introduction

Far infrared spectroscopy holds the promise to provide information about the conformation and structural characteristics of peptides and proteins, and thus bioinspired polypeptide based nano-materials.<sup>1-4</sup> If using a strong THz power source such as a synchrotron beam, far infrared spectroscopy provides reliable data in the low frequency domain, below 700  $\text{cm}^{-1}$ .<sup>3, 5, 6</sup> The prerequisite for using far-IR spectroscopy as a routine tool for structural analysis is an in-depth understanding of the conformation-dependence of the vibrations of the moieties that exhibit characteristic modes in this frequency range.

Due to the high conformational sensitivity of the far-IR modes that can result in shifts of more than 100  $\text{cm}^{-1}$ , the interpretation of experimental data is substantially less straightforward than that of mid-IR spectroscopy

(“fingerprinting” range); there are only very broad generalizations in existence about peak assignment in this region. The most important moieties with characteristic vibrational modes in the far-IR are the amide and carboxylic acid<sup>2, 7</sup>. Amide modes are of particular interest as these carry the structural information required to identify the conformation (folding) of polypeptides. Early studies used simple systems such as aliphatic amino acids and *N*-methyl acetamide that contains only one amide bond to identify the amide bands.<sup>8, 9</sup> Four amide modes are usually recognized in this wavenumber range: amide IV O-C-N bending<sup>10</sup>, usually in the range of 625-770  $\text{cm}^{-1}$ ; amide V out-of-plane N-H bending (640-800  $\text{cm}^{-1}$ );<sup>10, 11</sup> amide VI, out of plane C=O bending (530-610  $\text{cm}^{-1}$ );<sup>12, 13</sup> and amide VII skeletal torsion at 200  $\text{cm}^{-1}$ .<sup>14</sup> Not only do these modes overlap substantially, but they also couple to other moieties, and are also highly sensitive to structural strain.

Lyophilized samples are used in most far-IR studies to avoid interference from the hydration shell,<sup>15</sup> which is an acceptable reference state for most applications since bioinspired nanomaterials would be often used in the dry state. Importantly, the carboxylic acid is usually protonated in

<sup>a</sup>Department of Chemistry and Physics, La Trobe Institute for Molecular Science, La Trobe University, Melbourne, Australia

<sup>b</sup>School of Mathematical and Physical Sciences, University of Technology Sydney, Australia

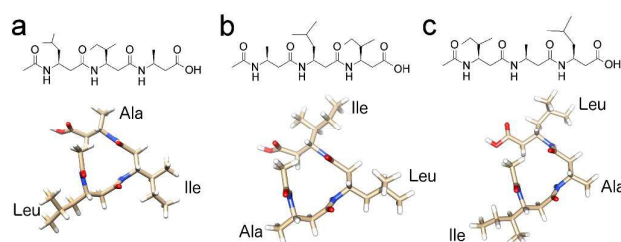


**Fig. 1** Symbolic (top) and energy minimized folding structures (bottom) of a) Ac- $\beta^3$ Leu- $\beta^3$ Ile- $\beta^3$ Ala, b) Ac- $\beta^3$ Ala- $\beta^3$ Leu- $\beta^3$ Ile, and c) Ac- $\beta^3$ Ile- $\beta^3$ Ala- $\beta^3$ Leu - the view is down the helix axis. For energy minimization an implicit water solvent model was used. The backbone retains the characteristic 14-helix geometry with only slight distortion.

lyophilized samples and exhibits a range of rocking, wagging and bending modes between 480 and 650  $\text{cm}^{-1}$  that directly overlap with the amide modes.<sup>16</sup> Low frequency peaks were reported at 247 and 328  $\text{cm}^{-1}$ .<sup>17</sup> Thus the carboxylic acid modes have to be taken into account when analyzing amide bands for conformational effects.

Side chains are also expected to have highly morphology-dependent vibrational modes in the low wavenumber range,<sup>18, 19</sup>  $\text{CH}_3$  bend is reported at  $\sim 100 \text{ cm}^{-1}$ .<sup>20</sup> Hence, polyglycine and polyalanine were used to study geometry dependent spectral features and hydrogen bond-related shifts in amide bands to avoid side chain interactions that complicate the interpretation of the spectra of larger peptides and proteins.<sup>15, 21-26</sup> However, as the far-IR range contains complex vibrational modes involving large groups of atoms in molecules that typically exhibit high conformational freedom, the outcome of these works underscores the issue that it is not possible to assign vibrational modes directly from a database; analysis has to be based on additional information, such as quantum mechanical calculations.<sup>27</sup> However, attempts to use density functional theory (DFT) calculations in the far-IR range for peak assignment yielded mixed results: while it is possible to model the vibration modes of small molecules in vacuum with good accuracy<sup>28</sup>, modelling polypeptides remains a challenge especially if using a high level of theory.<sup>29</sup> The limits to accurately predicting polypeptide vibrational modes is related to the high conformational flexibility of these molecules.<sup>29</sup>

A key issue of working with polypeptides is their inherently weak conformational stability; the related  $\beta^3$  peptides (where an additional carbon is present in the peptide backbone compared to naturally occurring  $\alpha$  amino acids) offer a solution.<sup>30, 31</sup>  $\beta^3$  peptides form stable helical structures with a pitch of 3.0-3.1  $\beta^3$  amino acids per turn.<sup>31</sup> We have described before that N-terminal acetylated  $\beta^3$ -peptides, including Ac- $\beta^3$ -tripeptides, self-assemble in a head-to-tail fashion into helical nanorods and hierarchical superstructures.<sup>32-34</sup> Here we use far-IR spectroscopy to analyze the conformation of the oligomeric form of Ac- $\beta^3$ Leu- $\beta^3$ Ile- $\beta^3$ Ala, Ac- $\beta^3$ Ile- $\beta^3$ Ala- $\beta^3$ Leu, and Ac- $\beta^3$ Ala- $\beta^3$ Leu- $\beta^3$ Ile (where Ac stands for acetyl,  $\beta^3$ Ala is the analogue of the naturally occurring alanine, and similarly for Leu and Ile) by correlating experimental far-infrared spectroscopy to DFT predictions of vibrational modes. We demonstrate the utility of the spectroscopic approach by

comparing the predicted vibrational spectra for implicit water solvent and vacuum, and show that the predictions clearly correspond to the experimental conditions. Importantly, this method is able to provide indirect structural information about self-assembled superstructures where crystallizing the material is not possible.

## 2 Materials and methods

**Materials.** The N-acetyl  $\beta^3$ -peptides Ac- $\beta^3$ Leucine- $\beta^3$ Isoleucine- $\beta^3$ Alanine (Ac- $\beta^3$ [LIA]), Ac- $\beta^3$ Alanine- $\beta^3$ Leucine- $\beta^3$ Isoleucine (Ac- $\beta^3$ [ALI]) and Ac- $\beta^3$ Isoleucine- $\beta^3$ Alanine- $\beta^3$ Leucine (Ac- $\beta^3$ [IAL]), were synthesized by our collaborators using solid phase synthesis as described previously.<sup>32</sup> In brief, peptides were synthesized from Fmoc-protected  $\beta$ -amino acids (GL Biochem, Shanghai, China) using standard Fmoc chemistry on Wang resin (0.9 mmol/g loading, GL Biochem). Peptides were cleaved from the resin with 2.5% v/v water and 2.5% v/v triisopropylsilane in TFA, dried and reconstituted in  $\text{H}_2\text{O}$ /acetonitrile (1:1) for HPLC purification (Agilent HP1200 system with a Vydac<sup>TM</sup> C18 preparative column) and lyophilization. The product was confirmed with Agilent 1100 MSD SL ion trap mass spectrometer in each case.

**Synchrotron far-IR experiments.** Transmission spectra for  $\sim 0.1$ - $0.2$  mg of each lyophilized peptide were collected at room temperature using Bruker IFS125/HR Fourier transform spectrometer with a He-cooled Si bolometer at the Australian Synchrotron THz/Far-IR beamline. Diamond or polyethylene cells were used at the focal point of the beam; the useful scan range with a resolution 2.0  $\text{cm}^{-1}$  was 50 to 650  $\text{cm}^{-1}$ , limited by the mylar beamsplitter and the polyethylene window on the bolometer, respectively. Each spectrum represents an average of ten experiments per sample each with a total of 200 scans collected.

**Density Functional Theory calculations.** The geometry of the three  $\beta$ -peptides was optimized using the Gaussian09 program in both vacuum and water solvent (implicit IEF method). Optimizations and vibrational analyses were performed using the B3LYP method with the 6-31G(d) basis set. Since in the low frequency range 6-31G(d) gives highly accurate predictions no scaling was applied.<sup>35, 36</sup> Importantly, DFT is accurate in predicting vibration energies (peak positions) but not peak intensities; accurately matching peak intensities has only been possible for small molecules in vacuum.<sup>28</sup>

DFT predicts vibrational modes with discrete eigen-frequencies (i.e. the peak width is zero). To correlate these predictions to experimental results Lorentzian peak profiles have been applied to these eigen-frequencies with 3.0% half-width using Molden 5.2 freeware. Graphs displaying the sum of the Lorentzian peaks were processed in Origin 7.0 (Originlab).

## 3 Results and discussion

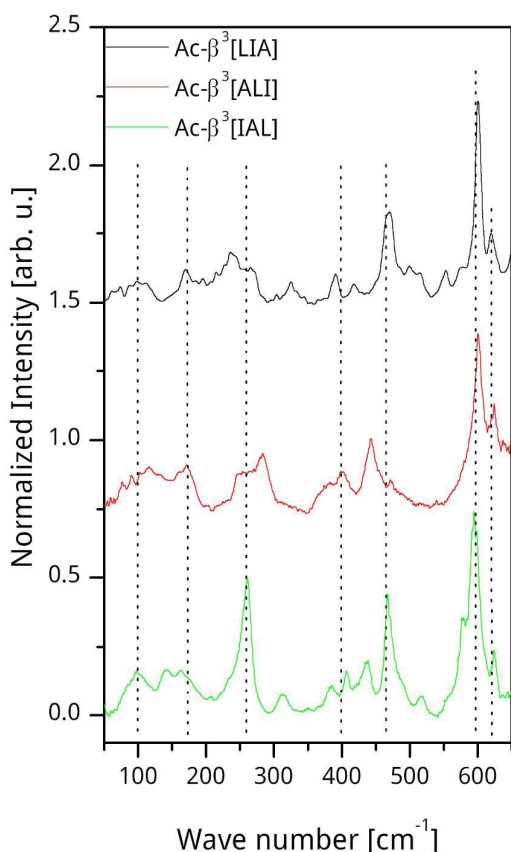


Fig. 2 Experimental far-IR spectra for the three beta peptides. Dotted lines indicate the common peak positions.

We studied three *N*-terminally acetylated isomeric  $\beta^3$ -tripeptides that only differ in the position of the  $\beta^3$ -amino acids in the sequence: Ac- $\beta^3$ Leu- $\beta^3$ Ile- $\beta^3$ Ala (Ac- $\beta^3$ [LIA]), Ac- $\beta^3$ Ile- $\beta^3$ Ala- $\beta^3$ Leu (Ac- $\beta^3$ [IAL]), and Ac- $\beta^3$ Ala- $\beta^3$ Leu- $\beta^3$ Ile (Ac- $\beta^3$ [ALI]). We have described the self-assembly and the various superstructures formed by these peptides before;<sup>32-34</sup> here we focus on the analysis of the far-IR spectra and the structural information obtainable through DFT vibrational analysis. The three peptides are depicted in (fig. 1). The conformation of all peptides is analogous to the 14-helix, the typical folding structure formed by substituted  $\beta^3$  peptides where 14 atoms form a single turn of the helical structure with a pitch of almost exactly 3.0 amino acids per turn. While the isomeric tri-peptides (fig. 1) lack the 4<sup>th</sup> residue and hence cannot have a true helical conformation, it was shown before that the head-to-tail self-assembly *via* the three amide bonds can stabilize the folding into a split ring.<sup>32-34</sup> In the figure, energy minimized structures are shown where the DFT calculations were started from a 14-helix conformation and an implicit solvent (dielectric constant 80.4) was used to emulate an aqueous environment. The implicit solvent also inhibits intramolecular hydrogen-bond formation; thus the energy minimized structure is determined by steric factors and angle strain, similar to the oligomeric form of the peptide. It is clear that upon energy minimization the monomers maintain similar overall conformation, with small changes in the dihedral angle

at the substituted backbone carbons. Importantly, this conformation is consistent with the self-assembled form where amide groups are aligned along the main helix axis. Experimental synchrotron far-IR spectra are shown in (fig. 2). The large peak at  $\sim 600\text{ cm}^{-1}$  is present for all three isomeric peptides. The peak has a nearly identical satellite in all cases at  $\sim 615\text{ cm}^{-1}$ . A common feature is also found at  $\sim 455\text{ cm}^{-1}$  that is shifted  $-10\text{ cm}^{-1}$  in case of Ac- $\beta^3$ [ALI]. There are several smaller peaks between  $390\text{--}450\text{ cm}^{-1}$ . A strong peak at  $250\text{ cm}^{-1}$  for Ac- $\beta^3$ [IAL] is split to two smaller peaks in both Ac- $\beta^3$ [ALI] and Ac- $\beta^3$ [LIA]. Finally, there are several peaks in the range  $100\text{--}170\text{ cm}^{-1}$  that are similar for Ac- $\beta^3$ [IAL] and Ac- $\beta^3$ [ALI], however, slightly attenuated in the case of Ac- $\beta^3$ [LIA]. Vibrational modes in this range have been assigned to amide and protonated carboxylic acid moieties.<sup>2, 7</sup> The amide modes of interest are amide IV O-C-N bending,<sup>10, 37</sup> usually in the range of  $625\text{--}770\text{ cm}^{-1}$ ; amide V out-of-plane N-H bending ( $640\text{--}800\text{ cm}^{-1}$ );<sup>10, 11</sup> amide VI, out of plane C=O bending ( $530\text{--}610\text{ cm}^{-1}$ );<sup>12, 13</sup> and amide VII skeletal torsion at  $200\text{ cm}^{-1}$ .<sup>14</sup> The highly chemical environment -dependent -OH bending mode of the carboxylic acid overlaps with the amide IV and V modes. Furthermore, not only do these modes overlap substantially, but they also couple to other moieties, and are also highly sensitive to structural strain. Side chains are expected to have highly morphology-dependent vibrational modes in the low wavenumber range that can be assigned to the peaks below  $300\text{ cm}^{-1}$ , however, these have not been identified in the literature thus far. Hence, DFT calculations have been performed to provide a more accurate assignment of the observed vibrational modes.

DFT calculations have been performed under two distinct conditions: in vacuum and in an implicit solvent (a constant dielectric space  $\epsilon = 80.4$ ). The main difference is expected to be in the energy-minimized structure, in particular the presence or absence of intramolecular hydrogen-bonding. The vacuum promotes hydrogen bonding, while the water environment disrupts weak hydrogen-bonding. Hence, the two calculations should not only show the stable geometries in these two environments but also reveal, in comparison to the experimental data, which conformation is most compatible with the geometry of the peptides used in the synchrotron far-IR experiments.

In the far-IR range traditional notions of modes and symmetry groups are of little use, given the coupling of the vibrations to large structural elements. Nevertheless it is possible to identify the moieties that have the largest displacement, and thus serve as the center of the vibrational modes. As discussed above, for the isomeric peptides Ac- $\beta^3$ [LIA], Ac- $\beta^3$ [ALI] and Ac- $\beta^3$ [IAL] the characteristic vibrations are expected to originate from the C-terminal carboxyl and the amide modes as well as the peptide backbone and side-chains.

The predicted vibrational modes of the DFT calculations in implicit solvent are detailed in Table 1 and (fig. 3). In general, the predicted modes (fig 3 bottom) are in remarkable agreement with the experimental spectra (fig. 3 top) even though intramolecular vibrational modes are not considered.

Table 1. DFT predictions of the main vibrational modes in a high dielectric implicit solvent medium. Only modes with good correlation to experimental results are listed.

Ac- $\beta^3$ [LIA] ( $\text{cm}^{-1}$ )		Ac- $\beta^3$ [ALI] ( $\text{cm}^{-1}$ )		Ac- $\beta^3$ [IAL] ( $\text{cm}^{-1}$ )		group <sup>a</sup>	type	coupled to
DFT	exp	DFT	exp	DFT	exp			
677	620	696	624	669	625	OH	oop	nearest -CH <sub>2</sub> -
656	600	669	601	658	595	OH	oop	backbone
		646	-	647, 639	584	OH	oop	NH(1) + two ends of the molecule
		581	-	659	578	OH	oop	nearest sidechain
543	552			553, 514	552, 518	NH(1)	oop	NH(2) + nearest sidechain
489	471	491	473	496	~490	NH(1)	twist	CH <sub>3</sub> <sup>b</sup> ; CH <sub>3</sub> + A <sup>c</sup> ; I <sup>d</sup>
578	575					NH(2)	oop	backbone
509	514	427	443	463	468	NH(2)	oop	NH(1) + I <sup>b</sup> ; NH(1) <sup>c</sup> ; A+L <sup>d</sup>
496	~497	466	~457	441	438	NH(2)	oop	L <sup>b</sup> ; backbone <sup>c</sup> ; backbone <sup>d</sup>
447	418	516	-	489	~490	NH(3)	oop	A <sup>b</sup> ; I + COOH <sup>c</sup> ; backbone <sup>d</sup>
DFT		exp						
band, ~200-250		band, ~220-290		CH <sub>3</sub>		twist		backbone
band, ~80-150		band, ~80-180		CH <sub>3</sub>		wag		backbone

The dominant vibration modes are out of plane (oop) bending for both OH and NH, coupled to other moieties as indicated. <sup>a</sup>The group with the largest displacement. <sup>b,c,d</sup>Moieties coupled to the core vibration of the given mode in Ac- $\beta^3$ [LIA], Ac- $\beta^3$ [IAL] Ac- $\beta^3$ [ALI] peptides, respectively, as a practical reference. Letters denote peptide sidechains: A, alanine; L, leucine; I, isoleucine.

Nevertheless the experimental spectra exhibit fewer peaks and some shifting of the bands is also observed. Vibrations related to the C-terminus are predicted in a band of 640-680  $\text{cm}^{-1}$  for Ac- $\beta^3$ [LIA] and Ac- $\beta^3$ [IAL]; the modes cover a broader,

581-696  $\text{cm}^{-1}$  range for Ac- $\beta^3$ [ALI]. The most intense mode is the out-of-plane bending of the OH that is coupled to backbone and side chain moieties, resulting in a series of peaks as a function of the local chemical environment. Overall, the position of these peaks is substantially higher than the dominant 600  $\text{cm}^{-1}$  peak observed experimentally; the shift towards lower energies is likely influenced by the damping effect from the self-assembly of the peptides that imposes narrower constraints on the conformation of the C terminus, with a potential contribution from intramolecular modes. The band of peaks in the range 400-550  $\text{cm}^{-1}$  is composed of distinct NH bending modes of all three amides, in all three peptides. By numbering the amide groups from the N-terminus, the modes are of NH(1), NH(2) and NH(3) depicted with brown, red and green colors, respectively, in (fig. 4). The energies of the three relatively uncoupled NH modes are remarkably similar to each other in all three peptides (Table 1), providing a good match to the 455  $\text{cm}^{-1}$ -centred band of the experimental spectra (figure 3 top). This agreement between theory and experiment suggests a largely preserved conformation that is consistent with the 14-helix folding geometry where the amides align with, and the side chains are perpendicular to, the main axis of the helix. Importantly, the experimental data show an even narrower spread of the side chain coupled amide modes that as a consequence do not separate into distinct peaks. Hence in the fully self-assembled state there are stronger conformational constraints than in the simulation, suggesting that the system is fully self-assembled without conformational variations. The side-chain coupled modes predicted at 514 and 553  $\text{cm}^{-1}$  in Ac- $\beta^3$ [IAL] likely correspond to the weaker peak at ~530  $\text{cm}^{-1}$  observed experimentally. The side chain coupled modes form a broad

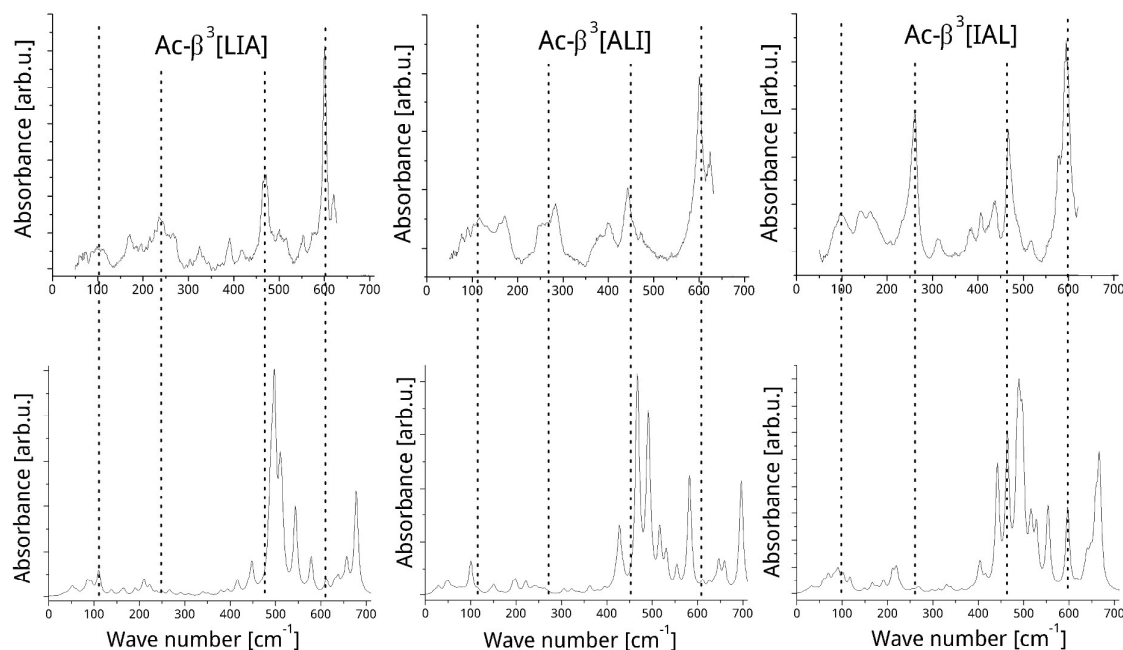
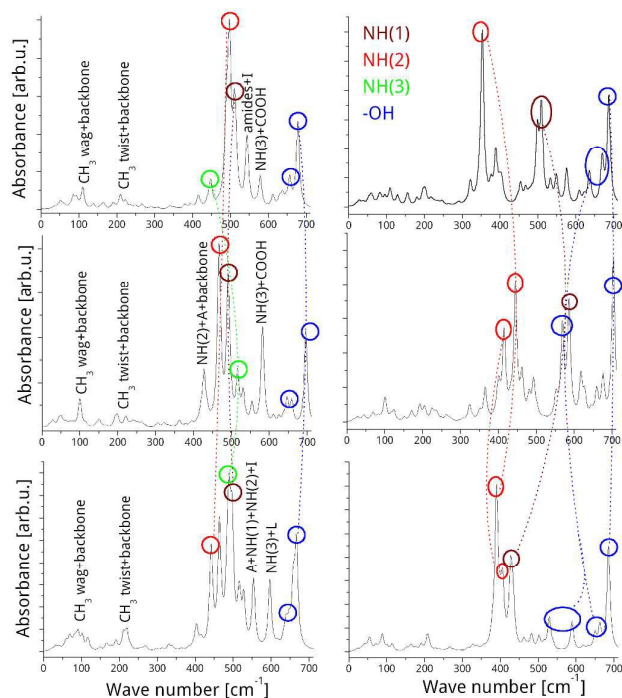


Fig. 3 Comparison of experimental (top) and predicted spectra (bottom) in implicit water solvent. The dotted lines indicate the peak positions in the experimental spectra. In the predicted spectra, the bands at ~470  $\text{cm}^{-1}$  and 100  $\text{cm}^{-1}$  are in good agreement, whereas the bands at 600  $\text{cm}^{-1}$  and ~250  $\text{cm}^{-1}$  appear at higher and lower energies, respectively, in the calculations.



**Fig. 4** Comparison of predicted vibrational spectra of the three isomeric peptides: top, Ac- $\beta^3$ [LIA]; middle, Ac- $\beta^3$ [ALI]; and bottom, Ac- $\beta^3$ [IAL] in implicit water solvent (left) and vacuum (right). Peaks of the same vibrational mode are indicated with distinct colours. Shifting of the peak position with folding is indicated with dotted lines.

peak in the experimental Ac- $\beta^3$ [LIA] spectrum in the 490-530 wavenumber range, however, do not give a distinct peak in the Ac- $\beta^3$ [ALI] spectrum.

The good agreement between the predicted and measured spectra allows for the analysis of the peaks in the 50-300 wavenumber range as well. While the identification of the moieties participating in these modes is even less straightforward than in case of the amide and carboxyl modes, it is possible to gain a view of “what moves”. The strong peaks observed experimentally in the proximity of 250  $\text{cm}^{-1}$  correspond well to a backbone “twist” involving the rotation of the  $\text{CH}_3$  moieties that is predicted as a series of peaks in a band of 200-250  $\text{cm}^{-1}$ ; the blue-shift in the experimental results indicates a confinement that is likely caused by the bundling of the peptide fibres as described before.<sup>33, 34</sup> The modes below 150  $\text{cm}^{-1}$  involve a  $\text{CH}_3$  wag coupled to “wobbling” of the backbone and the longer side chains. We note that comparison of solid-state vibrational spectra with calculations on isolated molecules should be taken *cum grano salis* because low frequency intermolecular modes may appear in this frequency region.<sup>19, 20, 38</sup>

Fig. 4 shows a comparison of the DFT predictions of the molecular vibrations in implicit solvent (left) and vacuum (right) in the 0-700  $\text{cm}^{-1}$  range. In the left-hand panels the assigned peaks are indicated. There are substantial differences between the two conditions. In case of the vacuum calculations, only the IAL spectrum shows a good resemblance to the experimental spectra, albeit with a poor quantitative agreement with the peak positions. It is possible, however, to



**Fig. 5** Energy minimized structures of the isomeric peptides in vacuum. Central helix region is shown. a) Ac- $\beta^3$ [LIA], b) Ac- $\beta^3$ [ALI] and c) Ac- $\beta^3$ [IAL]. Note the hydrogen bond between the C terminus and NH(1) in Ac- $\beta^3$ [LIA] and a hydrogen bond between NH(1) and NH(3) in Ac- $\beta^3$ [ALI]

identify the key differences and their possible causes in the molecular conformation.

In vacuum, the OH wag is observed at similar energies as in the case of the implicit solvent calculations, however, the backbone coupled modes are stronger and more widely spread. The highest intensity band is at 685-700  $\text{cm}^{-1}$  for a nearly pure OH bend (dashed blue line in fig. 4). Towards lower energies, Ac- $\beta^3$ [LIA] and Ac- $\beta^3$ [IAL] only show a series of weak peaks resulting from the OH wag coupling to the backbone and the nearest side chain; however, in case of Ac- $\beta^3$ [ALI] OH wag coupling to the backbone leads to an intense doublet at  $\sim 568$ -551  $\text{cm}^{-1}$  (blue line, fig. 4). The shift of the backbone coupled mode is the result of the structural strain introduced by a hydrogen-bond between the N-terminal (NH(1)) and the third amide (NH(3)) groups (fig.5) that lead to a twist of NH(1) and NH(3) from the near vertical position in the 14-helix geometry<sup>39-41</sup>. Although long and hence weak, this H-bond leads to a high-frequency NH out-of-plane bending mode of NH(1) in Ac- $\beta^3$ [ALI] at 585  $\text{cm}^{-1}$ . The out-of-plane NH bending of NH(1) is found at 426  $\text{cm}^{-1}$  in IAL and at  $\sim 500$   $\text{cm}^{-1}$  in case of Ac- $\beta^3$ [LIA] (brown colour, fig. 4). Importantly, Ac- $\beta^3$ [LIA] also exhibits an intramolecular hydrogen-bond, between NH(1) and the carboxyl group. Hence, the NH(1) mode is affected by the twisting of the amide and/or the coupling effect of the intramolecular hydrogen-bonding. The NH(2) modes were similar (red line, fig. 4). Importantly no clear NH(3) modes could be discerned.

Thus, the folding and intramolecular hydrogen-bonding is predicted to have a profound effect on the vibrational modes of these peptides. However, these spectra did not bear a high resemblance to the experimental results, hence it can be assumed that intramolecular hydrogen-bonding was absent in the lyophilized samples studied with far-IR spectroscopy. It has been shown previously that these peptides self-assemble into a fibrous superstructure, presumably closely following the 14-helix folding geometry of the  $\beta^3$  peptides.<sup>32-34</sup> Hence, the calculations should reflect this structure. Vibration spectra of the self-assembled superstructure cannot be modelled, however, a similar geometry can be imposed on the peptide monomers if the hydrogen-bonding is inhibited by increasing the dielectric constant of the environment.

## 4 Conclusions

It was conclusively demonstrated that synchrotron far-IR spectroscopic measurements provide a reliable fingerprint of the peptide folding in one-dimensional self-assembled

systems. DFT-based vibrational analysis of the monomers in the anticipated folding geometry offers a good match to the experimental spectra and thus it provides the means of peak assignment. We demonstrated the sensitivity of the spectra to peptide conformation by using DFT predictions under two different conditions: vacuum and an implicit high-dielectric solvent medium, where the energy minimization in vacuum alters the peptide conformation leading to predictions that do not agree with the experimental spectra. Therefore, our results open the way for using far-IR spectroscopy for structural analysis of polypeptide nanomaterials that is particularly useful in case of one- and two-dimensional materials where standard crystallographic analysis is not available.

### Acknowledgements

The authors acknowledge Mark Del Borgo for preparing the peptides; Marie-Isabel Aguilar and Patrick Perlmutter for their inspirational work on beta peptide design. This research was undertaken on the THz/Far-IR beamline at the Australian Synchrotron, Victoria, Australia and we would like to thank Dr Dominique Appadoo and Dr Joonsup Lee (VSCF, University of Sydney) for experimental assistance on this beamline.

### References

1. T. Ding, R. Y. Li, J. A. Zeitler, T. L. Huber, L. F. Gladden, A. P. J. Middelberg and R. J. Falconer, *Opt. Express*, 2010, **18**, 27431-27444.
2. T. Ding, A. P. J. Middelberg, T. Huber and R. J. Falconer, *Vib. Spectrosc.*, 2012, **61**, 144-150.
3. R. J. Falconer and A. G. Markelz, *J. Infrared Millim. Terahertz Waves*, 2012, **33**, 973-988.
4. R. J. Falconer, H. A. Zakaria, Y. Y. Fan, A. P. Bradley and A. P. J. Middelberg, *Appl. Spectrosc.*, 2010, **64**, 1259-1264.
5. N. Laman, S. S. Harsha, D. Grischkowsky and J. S. Melingery, *Biophys. J.*, 2008, **94**, 1010-1020.
6. K. Siegrist, C. R. Bucher, I. Mandelbaum, A. R. H. Walker, R. Balu, S. K. Gregurick and D. F. Plusquellic, *J. Am. Chem. Soc.*, 2006, **128**, 5764-5775.
7. D. F. Plusquellic, K. Siegrist, E. J. Heilweil and O. Esenturk, *ChemPhysChem*, 2007, **8**, 2412-2431.
8. L. Genzel, F. Kremer, A. Poglitsch and G. Bechtold, in *Coherent Excitations in Biological Systems*, Springer, 1983, pp. 58-70.
9. T. C. Cheam and S. Krimm, *J. Mol. Struct.*, 1986, **146**, 175-189.
10. J. Kong and S. Yu, *Acta Biochim. Biophys. Sinica*, 2007, **39**, 549-559.
11. J. Bandekar, *Biochim. Biophys. Acta*, 1992, **1120**, 123-143.
12. M. T. S. Rosado, M. Duarte and R. Fausto, *J. Mol. Struct.*, 1997, **410**, 343-348.
13. H. Tadokoro, Kobayash.M, Yoshidom.H, K. Tai and D. Makino, *J. Chem. Phys.*, 1968, **49**, 3359-&.
14. S. Dorr, U. Schade and P. Hellwig, *Vib. Spectrosc.*, 2008, **47**, 59-65.
15. R. Katakai, *J. Am. Chem. Soc.*, 1977, **99**, 232-234.
16. C. VogelWeill and A. Gruger, *Spectrochim. Acta, Pt. A: Mol. Biomol. Spectrosc.*, 1996, **52**, 1297-1310.
17. F. L. Jiang, I. Ikeda, Y. Ogawa and Y. Endo, *J. Oleo Sci.*, 2011, **60**, 339-343.
18. D. G. Allis, A. M. Fedor, T. M. Korter, J. E. Bjarnason and E. R. Brown, *Chem. Phys. Lett.*, 2007, **440**, 203-209.
19. M. R. C. Williams, D. J. Aschaffenburg, B. K. Ofori-Okai and C. A. Schmuttenmaer, *J. Phys. Chem. B*, 2013, **117**, 10444-10461.
20. Z. P. Zheng and W. H. Fan, *J. Biol. Phys.*, 2012, **38**, 405-413.
21. A. Trivella, T. Gaillard, R. H. Stote and P. Hellwig, *J. Chem. Phys.*, 2010, **132**, 10.
22. A. Matei, N. Drichko, B. Gompf and M. Dressel, *Chem. Phys.*, 2005, **316**, 61-71.
23. Y. Abe and S. Krimm, *Biopolymers*, 1972, **11**, 1817-1839.
24. Y. Abe and S. Krimm, *Biopolymers*, 1972, **11**, 1841-1853.
25. W. H. Moore and S. Krimm, *Biopolymers*, 1976, **15**, 2439-2464.
26. K. Itoh, Shimanou.T and M. Oya, *Biopolymers*, 1969, **7**, 649-658.
27. K. Itoh, A. Ikeda, T. Iwamoto and S. Nishizawa, *J. Mol. Struct.*, 2011, **1006**, 52-58.
28. S. A. Katsyuba, E. E. Zvereva and T. I. Burganov, *J. Phys. Chem. A*, 2013, **117**, 6664-6670.
29. J. Mahe, S. Jaeqx, A. M. Rijs and M. P. Gaijeot, *Phys. Chem. Chem. Phys.*, 2015, **17**, 25905-25914.
30. A. M. Bruckner, P. Chakraborty, S. H. Gellman and U. Diederichsen, *Angew. Chem. Int. Ed.*, 2003, **42**, 4395-4399.
31. R. P. Cheng, S. H. Gellman and W. F. DeGrado, *Chem. Rev.*, 2001, **101**, 3219-3232.
32. M. P. Del Borgo, A. I. Mechler, D. Traore, C. Forsyth, J. A. Wilce, M. C. J. Wilce, M. I. Aguilar and P. Perlmutter, *Angew. Chem. Int. Ed.*, 2013, **52**, 8266-8270.
33. R. S. Seoudi, M. P. Del Borgo, K. Kulkarni, P. Perlmutter, M. I. Aguilar and A. Mechler, *New J. Chem.*, 2015, **39**, 3280-3287.
34. R. S. Seoudi, A. Dowd, M. Del Borgo, K. Kulkarni, P. Perlmutter, M. I. Aguilar and A. Mechler, *Pure Appl. Chem.*, 2015, **87**, 1021-1028.
35. A. P. Scott and L. Radom, *J. Phys. Chem.*, 1996, **100**, 16502-16513.
36. J. P. Merrick, D. Moran and L. Radom, *J. Phys. Chem. A*, 2007, **111**, 11683-11700.
37. T. Miyazawa, T. Shimanouchi and S. I. Mizushima, *J. Chem. Phys.*, 1956, **24**, 408-418.
38. P. U. Jepsen and S. J. Clark, *Chem. Phys. Lett.*, 2007, **442**, 275-280.
39. T. L. Raguse, J. R. Lai and S. H. Gellman, *Helv. Chim. Acta*, 2002, **85**, 4154-4164.
40. E. Vaz, W. C. Pomerantz, M. Geyer, S. H. Gellman and L. Brunsveld, *ChemBioChem*, 2008, **9**, 2254-2259.
41. D. H. Appella, L. A. Christianson, D. A. Klein, D. R. Powell, X. L. Huang, J. J. Barchi and S. H. Gellman, *Nature*, 1997, **387**, 381-384.